Journal of the Optical Society of America B
OPTICAL PHYSICS

Influence of spatial dispersion on surface plasmons, nanoparticles, and grating couplers

Armel Pitelet,[1] Nikolai Schmitt,[2] Dimitrios Loukrezis,[3] Claire Scheid,[2] Herbert De Gersem,[3] Cristian Ciracì,[4] Emmanuel Centeno,[1] and Antoine Moreau[1,*]

[1]Université Clermont Auvergne, CNRS, SIGMA Clermont, Institut Pascal, F-63000 Clermont-Ferrand, France
[2]Université Côte d'Azur, Inria, CNRS, LJAD, 06902 Sophia Antipolis, France
[3]Institute for Accelerator Science and Electromagnetic Fields (TEMF), Technische Universität Darmstadt, 64289 Darmstadt, Germany
[4]Center for Biomolecular Nanotechnologies, Istituto Italiano di Tecnologia, 73010 Arnesano (LE), Italy
*Corresponding author: antoine.moreau@uca.fr

Received 21 May 2019; revised 6 September 2019; accepted 12 September 2019; posted 13 September 2019 (Doc. ID 368168); published 10 October 2019

Recent experiments have shown that spatial dispersion may have a conspicuous impact on the response of plasmonic structures. This suggests that in some cases, the Drude model should be replaced by more advanced descriptions that take spatial dispersion into account, such as the hydrodynamic model. Here, we show that nonlocality in the metallic response affects surface plasmons propagating at the interface between a metal and a dielectric with high permittivity. As a direct consequence, any nanoparticle with a radius larger than 20 nm can be expected to be sensitive to spatial dispersion, whatever its size. The same behavior is expected for a simple metallic grating allowing the excitation of surface plasmons, just as in Wood's famous experiment. Finally, we carefully set up a procedure to measure the signature of spatial dispersion precisely, leading the way for future experiments. Importantly, our work suggests that for any plasmonic structure in a high-permittivity dielectric, nonlocality should be taken into account.

https://doi.org/10.1364/JOSAB.36.002989

1. INTRODUCTION

For more than a century now, Drude's model [1], coupled to Maxwell's equations [2], has been able to describe very accurately the optical response of metals, even for quite extreme geometries [3–7]. Many advanced theories describing metal-vacuum interfaces [8,9] have been developed during the second half of the 20th century, especially with the development of electron energy loss spectroscopy (EELS), which provided experimental data to better ground theoretical discussions [10–12]. These new approaches were able to take into account complex phenomena, such as spatial dispersion or electron spill-out, and allowed one to better understand the success of Drude's model. It turns out in fact that Drude's theory is the zeroth order approximation of all more advanced descriptions introduced later on. All these studies, however, seemed to conclude that spatial dispersion and spill-out have a limited impact [13–16] on surface plasmons (SPs), such that optical experiments were not likely to show any difference from Drude's predictions [17–19]. Moreover, because most resonances in metallic structures can actually be explained as cavity resonances of some sort for SPs, it has become widely accepted that plasmonic resonances could be very accurately described by Drude's model. For decades, then, there has not been any urge to adopt advanced descriptions of the response of metals in plasmonics. Only in the case of metallic clusters, due to the extremely small size, were spatial dispersion and spill-out expected to play a significant role, requiring the most advanced descriptions [13,20–22].

However, a recent experiment with film-coupled nanoparticles showed that the frequency of the resonance of modes that are localized in small volumes (on the order of 1 nm^3) is simply not correctly predicted by Drude's model, whereas the linearized hydrodynamic model [23] in its simplest formulation (the Thomas-Fermi approximation) seemed to be accurate enough. This is the case even with optical excitation and relatively large metallic particles. This can be linked to the fact that the small gaps between the nanoparticle and the metal support a gap-plasmon—a guided mode that is particularly sensitive to spatial dispersion because it has a very large wavevector [24–28], whatever the frequency. This allows one to better understand why small gaps, which are more and more common in plasmonics [3,5,29–31], may require more advanced descriptions of the metallic response. Furthermore, this explains why the hydrodynamic model, despite its well-documented deficiencies [32], is probably a good replacement for Drude's model in plasmonics [33,34]: high wavevector plasmonic modes enhance spatial dispersion effects [26–28], but not the impact of the spill-out,

especially since noble metals present a high extraction work. The spatial dispersion that arises from the repulsion between free electrons inside the metal is taken into account accurately by a hydrodynamic model, which presents in addition the advantage of being relatively easy to implement numerically [35–38].

Here, we show that the impact of spatial dispersion on the SP propagating at the interface between a metal and a dielectric is enhanced when the refractive index of the dielectric is large. We show, as a direct consequence, that even large nanoparticles can be expected to be sensitive to nonlocality and that, using a grating coupler, it is theoretically possible to estimate the main parameter of the linearized hydrodynamic model in a situation where other more complex phenomena can be ruled out. We underline that such a well-controlled setup differs strongly from previous experiments that all involved chemically synthesized nanoparticles [20,39–41] whose geometry cannot always be fully controlled.

2. SURFACE PLASMON

In this first part, we study the influence of spatial dispersion on a SP propagating along a metal-dielectric interface (especially for dielectrics with high refractive indices). A SP can be seen as current loops propagating beneath the surface of a metal. Such a phenomenon is accompanied by an electromagnetic field in the metal (with relative permittivity ε_m) and in the dielectric (with relative permittivity ε_d), which is transversely evanescent in both media due to the fact that its effective index $n_{\text{eff}} = \frac{k_{\text{SP}}}{k_0}$, where k_{SP} is the wavevector of the SP and $k_0 = \frac{\omega}{c}$ is the wavevector in vacuum, is always larger than the refractive index of the dielectric medium.

First, neglecting losses, the dispersion relation can be written as

$$n_{\text{eff}} = \sqrt{\frac{\varepsilon_d \varepsilon_m}{\varepsilon_d + \varepsilon_m}}, \tag{1}$$

where we assumed a simple Drude model $\varepsilon_m = 1 - \frac{\omega_p^2}{\omega^2}$. In this case, the curve of a SP has a horizontal asymptote at $\omega_{\text{SP}} = \frac{\omega_p}{\sqrt{1+\varepsilon_d}}$. It is, however, unrealistic to neglect the losses inside the metal because the frequency ω_{SP} is usually in a wavelength range, the UV, where the interband transitions make the metal highly lossy. As a consequence, a bend-back can be seen on the dispersion curve of the SP, which thus never reaches very high wavevectors (see local dispersion curves in Fig. 1).

However, when the permittivity of the dielectric increases, the frequency ω_{SP} decreases. At the same time, losses due to the interband transitions can be expected to be low enough as to enable a support of high wavevector SPs. Such modes are more likely to be sensitive to spatial dispersion [24].

In order to take nonlocality into account, we rely on the linearized hydrodynamic model for the free electrons, already introduced in previous works [35,43–48]. The electric current $\mathbf{J}$ inside the metal is linked to the electric field $\mathbf{E}$ by

$$-\beta^2 \nabla(\nabla \cdot \mathbf{J}) + \ddot{\mathbf{J}} + \gamma \dot{\mathbf{J}} = \varepsilon_0 \omega_p^2 \ddot{\mathbf{E}}, \tag{2}$$

where ω_p is the plasma frequency, ε_0 the vacuum permittivity, γ the damping factor, and β the nonlocal parameter. The β factor represents the increase in internal pressure in the electron gas due to exchange interaction and Coulomb repulsion. There are actually several theoretical expressions for this parameter [49]. We rely on the experimental data available [39,40], which consistently point to a value of $\beta = 1.35 \times 10^6 \ \frac{\text{m}}{\text{s}}$. Finally, the electric current inside the metal can always be considered as an effective polarization $\mathbf{P}_f$ due to the free electrons and is then given by $\dot{\mathbf{P}}_f = \mathbf{J}$. In that framework, the metal can then be described as a nonlocally polarizable medium.

We use accurate material parameters [42] that allow a distinction between the response of the free electrons, which is subject to spatial dispersion, and the response of bound electrons, which can be considered to be purely local [50]. In the following, the metal is always assumed to be silver, which is favorable since silver is less lossy than gold. The total metal polarization reads then $\mathbf{P} = \mathbf{P}_f + \mathbf{P}_b$, where $\mathbf{P}_b = \varepsilon_0 \chi_b \mathbf{E}$ with χ_b being the local susceptibility associated with the bound electrons. In order do obtain χ_b, we fit the experimental data of silver permittivity with a generalized dispersion model based on Padé series [51] (which is sufficient to perform nonlocal time-domain simulations) and subtract the local Drude contribution χ_f. Throughout this work, we rely on the DIOGENeS [52] Discontinuous Galerkin Time-Domain (DGTD) suite [37]. Finally, we consider additional boundary conditions that are both the most natural (vanishing normal component of the polarization current $\mathbf{J}$ at the metal boundary, thus forbidding free electrons to escape the metal) and the most conservative (they reduce the impact of nonlocal effects) [24]. Since the current is proportional to the effective polarization in the metal due to the gas of free electrons, this boundary condition, used all througout the present work, can be written as $\mathbf{P}_f \cdot \mathbf{n} = 0$ at the surface of the metal.

We first study the influence of nonlocality by considering the dispersion relation of a SP propagating along a perfectly plane dielectric-metal interface. The calculations done in [24] show that this relation can be written as

$$\frac{k_m}{\varepsilon_m} + \frac{k_d}{\varepsilon_d} - i\Omega = 0, \tag{3}$$

where $k_j = \sqrt{\varepsilon_j k_0^2 - k_{\text{SP}}^2}$, $j = \text{m}, \text{d}$ are the vertical components of the SP wavevector, and Ω is the parameter including β and thus taking nonlocality into account. Presuming $\Omega = 0$ allows one to retrieve the usual dispersion relation for SPs, the $k_j = k_j' + ik_j''$ being here essentially imaginary ($k_j'' \gg k_{j'}$). We underline that the above expression is only apparently different from [24] because we use the wavevectors k_j directely in the expressions instead of the $\kappa_j = \sqrt{k_{\text{SP}}^2 - \varepsilon_j k_0^2}$ as done in [24]. The expression of Ω for the boundary conditions we use is

$$\Omega = \frac{k_{\text{SP}}^2}{\sqrt{k_{\text{SP}}^2 + \left(\frac{\omega_p^2}{\beta^2}\right)\left(\frac{1}{\chi_f} + \frac{1}{1+\chi_b}\right)}} \left(\frac{1}{\varepsilon_m} - \frac{1}{1+\chi_b}\right). \tag{4}$$

As can be seen from Eq. (4), the parameter Ω is roughly proportional to the square of k_{SP}, which clearly indicates that the higher the wavevector, the higher the impact of nonlocality. Figure 1 shows local and nonlocal SP dispersion curves for different values of the dielectric permittivity ε_d ranging from 1 to 10. We can easily see that, for a fixed frequency, an increasing ε_d pushes the SP towards higher n_{eff}, and thus causes the SP to be more

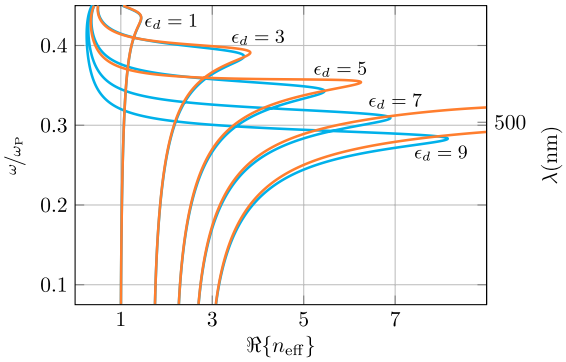

Fig. 1. Surface plasmon dispersion curves [see relation Eq. (3)] along a single dielectric-Ag interface, assuming material parameters for silver [42]. The effective index $n_{\text{eff}} =$ is defined by $\frac{k_{\text{SP}}}{k_0}$. The permittivity of the dielectric ε_{d} ranges from 1 (most left) to 9 (most right) with a step size 2. The blue lines correspond to the local dispersion ($\Omega = 0$) and the orange ones to nonlocal dispersion ($\Omega \neq 0$).

sensitive to nonlocality. The leftmost curve, obtained using air as the dielectric ($\varepsilon_{\text{d}} = 1$), clearly shows that the effective index n_{eff} is too small to show any impact of nonlocality. However, after a certain ε_{d} value, the characteristic bend-back occurring at the SP frequency ω_{SP} disappears just when spatial dispersion is taken into account.

This corresponds exactly to a recent theoretical study [25] that shows that an artificial decrease in metallic losses can induce exactly the same behavior on the dispersion curves of plasmonic guided modes. This occurs when the impact of nonlocality overcomes the influence of the metallic losses.

The impact of the dielectric's permittivity overcomes the one of losses for two reasons. First, as explained above, increasing ε_{d} lowers ω_{SP} and thus takes the frequency away from the interband transitions. Additionally, a higher dielectric permittivity *directly* gives to the SP a higher n_{eff} and thus enhances the influence of spatial dispersion, leading to a large impact of nonlocality even well below ω_{SP}.

However, when the real part of the effective index shown in Fig. 1 is especially high, the imaginary part is very large too, making the mode impossible to excite. This means reaching out for the highest wavevectors may not be the best strategy to observe nonlocal effects.

We underline that, despite extensive studies on nanoparticles, such a behavior of the SP has seemingly not been reported previously. Straightforwardly, this suggests that nonlocality will have an impact on (i) the resonances of *relatively large* nanoparticles of noble metals (with a diameter well above 20 nm, as they can be considered as resonant cavities for the surface plasmon) and (ii) SP grating couplers very similar to the canonical experiment of Wood [53], provided the grating is buried in high-index dielectrics.

3. NANOPARTICLES

The resonance of large metallic nanoparticles can be interpreted as cavity resonances for the surface mode with a resonance condition [54], which can be written as

$$2\pi R = m\frac{\lambda_0}{n_{\text{eff}}} \tag{5}$$

or simply as $k_{\text{SP}} = \frac{m}{R}$, where R is the radius of the particle. Such a condition is strictly valid only (i) for a cylinder instead of a sphere and (ii) if the curvature of the particle can be neglected, which is almost never the case. However, this condition being roughly valid even for spherical nanoparticles instead of cylinders [54,55], it allows one to understand that if the wavevector of the SP is influenced by nonlocality, the resonance frequencies of a nanoparticle should be influenced as well, *irrespective of its size*.

For decades now, the community has actually focused on nanoparticles with a diameter much smaller than 20 nm [20,41], hoping that enhanced nonlocal effects would take place—since spatial dispersion is linked to supplementary pressure terms in the description of electron gas [49,56]. However, with very small nanoparticles, (i) other effects such as spill-out [22,33,57,58] kick in, and (ii) the geometry of the nanoparticles is not well controlled [20,41]. Given the relatively poor agreement between experiments and the prediction of the hydrodynamic model [41,59], it seems difficult to consider the hydrodynamic model to be sufficient at such small scales. It may even be a little bit early to introduce further improvements of the hydrodynamic model [60] based on these results. The simple analysis above suggests that larger nanoparticles buried in a high-permittivity medium could actually be a better setup to test the hydrodynamic model.

In order to further strengthen this analysis, we used Mie theory [54,55] and adapted the formalism proposed by Ruppin [61] for metallic cylinders, for which formula (5) is the most relevant. We use the most realistic material parameters possible [42] and the supplementary condition considered above for the SP. This boundary condition, $\mathbf{P}_{\text{f}} \cdot \mathbf{n} = 0$, leads to the following relation [24]:

$$\left(\mathbf{E} - (1+\chi_b)\frac{\beta^2}{\omega_p^2}\nabla(\nabla\cdot\mathbf{E})\right)\cdot\mathbf{n} = 0, \tag{6}$$

where $\mathbf{n}$ is the unitary vector normal to the surface of the metal. When the field is decomposed on the cylindrical harmonics, the Mie coefficients [61] are

$$a_n = \frac{\sqrt{\epsilon_d}J_n(k_d R)(J_n'(k_m R)+\alpha_n) - \sqrt{\epsilon_m}J_n(k_m R)J_n'(k_d R)}{\sqrt{\epsilon_m}H_n'(k_d R)J_n(k_m R) - \sqrt{\epsilon_d}H_n(k_d R)(J_n'(k_m R)+\alpha_n)}, \tag{7}$$

where

$$\alpha_n = \frac{\frac{n^2}{k_m R^2}J_n(k_L R)J_n(k_m R)}{-k_L J_n'(k_L R) + (1+\chi_b)\frac{\beta^2}{\omega_p^2}\beta_n} \tag{8}$$

and

$$\beta_n = k_L^3 J_n'''(k_L R) + \frac{k_L^2}{R}J_n''(k_L R) - \frac{k_L}{R^2}(n^2+1)J_n'(k_L R) + \frac{2n^2}{R^3}J_n(k_L R) \tag{9}$$

with $k_m = \sqrt{\epsilon_m}k_0$, $k_d = \sqrt{\epsilon_d}k_0$, and

$$k_L = \sqrt{-\frac{\omega_p^2}{\beta^2}\left[\frac{1}{1+\chi_b} + \frac{1}{\chi_f}\right]}. \tag{10}$$

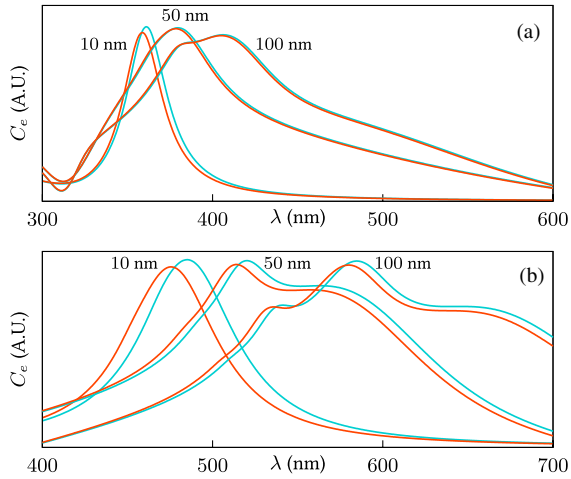

Fig. 2. Local (blue) and nonlocal (orange) absorption for a cylinder cross section of radius (from left to right) $R = 10$ nm, 50 nm, and 100 nm as a function of the impinging wavelength λ for a p-polarized incident wave (**H** parallel to the cylinders) using (a) water or (b) TiO_2 as dielectric. The theoretical blue shifts (for the maxima) are from left to right 2.1 nm, 1.2 nm, and 0.9 nm in (a) and 9.3 nm, 6.0 nm, and 4.8 nm in (b).

We then compute the extinction cross section as

$$C_e = -\frac{2}{k_d R}\sum_{n=-\infty}^{\infty}\Re(a_n). \tag{11}$$

Because expression (7) is numerically unstable when β tends to zero, one has to take $\alpha_n = 0$ to find the local predictions using the same formula.

We have computed the local and nonlocal response of nanoparticles with different sizes when they are in water (as is common) or in TiO_2 (see Fig. 2). The latter is a good choice to enhance the influence of spatial dispersion because of its high refractive index. Its permittivity ε_{TiO_2} is described by a generalized dispersion model fitted to experimental data corresponding to thin films of TiO_2 grown by atomic layer deposition [62]. This results in a real part of the refractive index of TiO_2 comprised between 2.25 and 2.5 over a wavelength spectrum ranging from 2000 nm to 400 nm. The extinction coefficient is on the order of 10^{-7}.

In water, nonlocality has a noticeable impact only for a radius approaching 10 nm, whereas in TiO_2, nonlocality tends to blue shift all the resonances of more than 4.8 nm in wavelength even for a radius of 100 nm. We stress here that a high-index dielectric is able to sufficiently enhance the magnitude of the nonlocal effects to make it observable on the response of particles/cylinders five times larger than the ones usually considered by the community. This should be enough to rule out any other effect such as the spill-out, and with such a large size, the geometry of the nanoparticles is better controlled—or the nanoparticles could even be probed individually [55,59].

4. GRATING COUPLER

We now discuss the structure shown in Fig. 3(a), which is a simple 1D metallic grating buried in a high-index dielectric

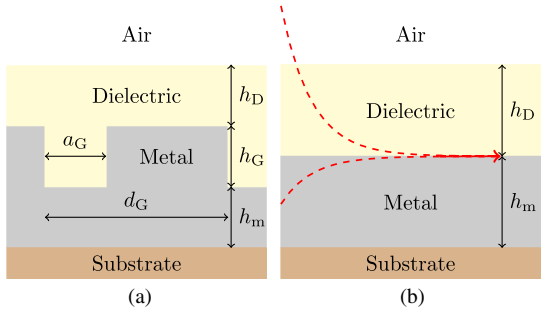

Fig. 3. (a) Schematic representation of a grating coupler. (b) Schematic representation of a SP propagating along a dielectric-metal interface, taking the finite height of the dielectric into account. The red dashed line illustrates the SP's magnetic profile. While the SP propagates along the dielectric-metal interface, the upper evanescent tail extends into air, but the lower one does not extend into the substrate, allowing one to neglect it in computations.

with infinite extent in the lateral directions. Normal incident illumination is assumed from the top, and we recover the zeroth reflected order for a broadband spectrum of the incident wavelength. In such a simple configuration, many diffraction orders, including evanescent ones, are excited.

For the m-th order, and since we consider only *normal incidence* here, the coupling condition to the SP can be simply written as

$$k_{SP} = m\frac{\lambda}{d_G}, \tag{12}$$

where λ is the wavelength, m the diffraction order, and d_G the grating pitch. Such a relation is valid only for a very shallow grating when the surface mode can be considered undisturbed. It is equivalent to assuming that the spatial periodicity of the grating is a multiple of the periodicity of the SP. Such a condition is proper to the periodicity of the structure [63] and thus is expected to be valid whether spatial dispersion (which will modify k_{SP}) is taken into account or not. This allows us to find the wavelength $\lambda_{c,m}$ for which the grating is able to excite the SP:

$$\lambda_{c,m} = \frac{\Re(n_{eff})}{m}d_G, \tag{13}$$

where $n_{eff} = \frac{k_{SP}}{k_0}$ is the SP effective index.

Each time this condition is satisfied, a dip due to the excitation of a SP will appear in the reflectivity. Spatial dispersion should cause blue shifts of the resonances with respect to a fully local approach because the effective index is always smaller when nonlocality is taken into account. We define this blue shift as the positive quantity $\Delta\lambda_{c,m} = \lambda_{c,m}^{local} - \lambda_{c,m}^{nonlocal} \propto n_{eff}^{local} - n_{eff}^{nonlocal}$. As the different resonances correspond to different orders being coupled to the SP, the corresponding wavevectors will be different, and thus the impact of spatial dispersion will change from one resonance to another. To better understand the impact of nonlocality on the resonances, it is crucial to be able to identify them, hence the interest in the relation Eq. (13). We have thus taken the finite thickness of the dielectric layer into account by computing the properties of the guided mode of the non-corrugated structure [see Fig. 3(b)] using an open-access

numerical tool [36,64]. Aiming for a proper interpretation of the resonances, we have then carefully increased the depth of the grating, in order to allow a thorough physical discussion (see Fig. 5). We use rigorous coupled-wave analysis (RCWA) [65,66] for these simulations.

A. Parameters of the Grating Coupler

1. Materials

Although we restrict ourselves to silver in the scope of this work, we underline that gold or any other metal and even semiconductors [67] (claiming an equivalent electronic mean free path [68]) could have been used and would have led to the same conclusions. Again, in order to observe the largest possible effects, we consider TiO_2 as a high-permittivity dielectric with very low absorption. It could be possible to consider other materials with an even higher refractive index, such as silicon for instance. The losses of these materials would, however, force us to consider higher wavelengths, further away from the plasma frequency, where nonlocality has a smaller impact—but for which their high refractive index could potentially compensate.

2. Thickness of the Dielectric and Metallic Layer

We have taken $h_m = 150$ nm for the thickness of the metallic layer, thus being several times thicker than the skin depth and ensuring that the substrate does not play any significant role.

The thickness of the dielectric h_D layer is a distinctly more crucial parameter. In order to excite a SP with the highest possible wavevector, a dielectric of the highest possible thickness would be desirable. However, since the dielectric layer is finitely thick, increasing h_D leads to a higher number of classical guided modes. That hinders a clear interpretation of the resonances or renders it even impossible. Luckily, since we are considering the excitation of high-wavevector guided modes that show a fairly low vertical extension, a thickness of $h_D = 85.0$ nm turns out to be a good trade-off. No other guided mode than the SP exists for this choice of h_D in most of the spectrum.

Figure 4(a) shows the dispersion curve for a mode propagating at an air-TiO_2-Ag interface for $h_D = 85$ nm with or without spatial dispersion. Obviously, the difference in the dispersion curve of the SP at a TiO_2-Ag interface is small. The impact of nonlocality is clearly the same, and the bend-back disappears.

3. Grating Pitch

Using the coupling condition Eq. (13) and the local and nonlocal dispersion curves as shown in Fig. 4(a), a raw estimation of the blue shift due to spatial dispersion can be made. Figure 4(b) shows the expected blue shift for different diffraction orders and sweeps over the grating periodicity d_G. The higher the diffraction order, the higher the wavevector of the excited SP—which leads to an increased impact of nonlocality. We have finally chosen a pitch length of $d_G = 500$ nm according to a maximum of the predicted blue shift of about 5.5 nm for $m = 5$. Keeping the pitch below the shortest working wavelength guarantees that only the zeroth order propagates, even if the evanescent orders of diffraction are coupled to the SP. In other words, all of the non-reflected light must be absorbed by the guided modes along the structure.

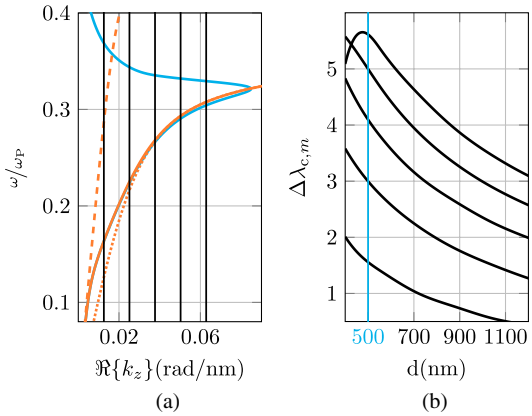

Fig. 4. (a) Dispersion relation of a SP propagating at an air-TiO_2-Ag multilayer. Local results are in blue, and nonlocal ones are in orange. For comparison, the two dashed lines are the nonlocal dispersion relations, respectively, for an Air-Ag interface (left) and a TiO_2-Ag interface (right). The black vertical lines indicate the coupling condition given by Eq. (13) for a grating pitch of 500 nm considering the five first diffraction orders (1 to 5 from left to right). (b) Estimation of the blue shift $\Delta\lambda_{c,m}$ as a function of the grating pitch d_G. m varies 1 to 5 (bottom to top).

4. Groove Width and Grating Thickness

The determination of the two remaining geometrical parameters, i.e., the groove a_G and the grating thickness h_G, is less straightforward. We have to establish a trade-off, such that the excitation of the SP for different orders of diffraction can be done efficiently without perturbing the guided mode too much. In order to avoid gap plasmons to build up in the slits [69], a large enough a_G value is needed. We choose $a_G = \frac{1}{3}d_G$ here. Starting from $h_G = 2$ nm, we have increased the grating depth until an efficient coupling to the SP mode was found—we relied on a pure RCWA method [65,66] to adjust this parameter.

It is easy to associate a diffraction order m for most of the resonances supported by the grating described above (see Fig. 5). However, starting from almost zero and progressively increasing the height h_G, the resonance that we first attributed to be of order $m = 1$ exhibits a splitting (see Fig. 5).

The field maps in Fig. 5 clearly show that one of the resonances corresponds to a cavity-like resonance, which is entirely located in the grooves of the grating, i.e., it is reflected back and forth horizontally. The other resonances are cavity resonances of SPs that propagate on top of the grating and are reflected by the edges of the metal. We label those resonances with 1b (where "b" stands for "bottom") and 1t (where "t" stands for "top"), respectively. Since the thickness of the dielectric is different for both kinds of plasmons, their wavevector cannot be the same, therefore the splitting. We finally chose to take $h_G = 68$ nm.

B. Influence of Nonlocality on Grating Reflectivity

Now that the grating has been designed and its physics is well understood, we use software taking spatial dispersion into

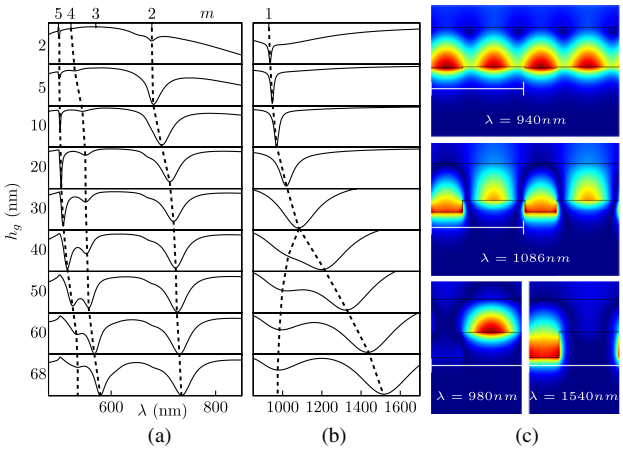

Fig. 5. (a) Reflectivity of the grating illuminated in normal incidence for different values of h_G computed using a local RCWA for $\lambda \in [480, 850]$ nm. (b) Reflectivity of the grating for different values of h_G for $\lambda \in [850, 1700]$ nm. Each vertical coordinate system has been chosen to maximize visibility. The horizontal one is kept constant from top to bottom. (c) Magnetic field amplitudes illustrating the splitting of diffraction order 1 into two sub-orders. The corresponding (h_G, λ) couples (in nm) are from top to bottom: (2,940), (30,1086), and (68,980) on the left and (68,1540) on the right.

account in order to assess its influence on the reflectivity of the grating. This is necessary, since analytical solutions do not exist anymore, and we have to rely on a numerical algorithm. Here, we use a DGTD method for the simulations of the grating. The result is shown in Fig. 6 for wavelengths ranging from $\lambda = 500$ nm to $\lambda = 2000$ nm. The small discrepancy between local DGTD and RCWA is due to a known problem of the latter in very peculiar conditions [70] and occurs only far off the resonances. We can clearly identify five dips due to SP excitation corresponding to four diffraction orders, the first order being split as discussed above. The results show a considerable influence of the spatial dispersion, which is significantly stronger than what has been predicted theoretically. This can be attributed to the grating itself and to the shift of the resonances towards large wavelengths (and larger wavevectors for the SP). The resonances linked to the diffraction orders $m = 4$ and $m = 2$ (see inset in Fig. 6) experience blue shifts of, respectively, 1.8 nm and 6.5 nm compared to the local prediction. Especially for $m = 2$, this is clearly higher than the expected shift of 3 nm [see Fig. 4(b)]. For $m = 4$, the shift is slightly smaller than expected. Because this mode is excited for a lower wavelength, it presents an effective index with a higher imaginary part. The field maps show that the mode is more localized in the dielectric than in the metal, resembling a mode that would be guided in the dielectric layer. This hybridization makes the mode less sensitive to nonlocality than the second-order mode, which propagates much closer to the metal.

Finally, we can identify two wavelength bands of interest. The first one for $\lambda = [550, 800]$ nm (see inset) shows the highest difference between local and nonlocal simulations. It comprises two blue shifted diffraction orders, and the whole response between the two is also clearly affected by nonlocality—making this regime a good choice to estimate the parameter β. The second region of interest is the rightmost part in Fig. 6 for $\lambda = [800, 2000]$ nm. It comprises the two suborders $1t$ and $1b$, which are less sensitive to nonlocality. For this reason, we believe that this region is not useful to probe nonlocality, but well suited for a geometrical parameter characterization. We have to keep in mind that any estimation of β relies merely on a comparison between material models. Such comparisons are very sensitive to the geometrical parameters. Since we are trying to measure discrepancies on the order of 1% of the wavelength, we must ensure that nonlocality will not be concealed by uncertainties on local parameters.

5. TELEMETRY AND PARAMETER ESTIMATION

In the previous section, we have theoretically predicted that the metallic grating that we have designed is sensitive to nonlocality. The goal of the present section is to present the challenges that would have to be faced by experimentalists and to propose a methodology relying on the solution of inverse problems and uncertainty quantification (UQ), which could be used to assess realistically the presence of nonlocality and to estimate the crucial β parameter.

In order to take into account the fact that, whatever the geometry and the imperfections of the grating, the spectra will be noisy, we have generated an artificial but realistic reflectance spectrum. We use nonlocal simulations and then add a noise whose characteristics are similar to actual experimental spectra provided by experimentalists [71]. The noise has been chosen with a correlation length of 0.001 nm and a maximum difference of 0.04 with the original, unperturbed spectrum. We have then tested whether the parameters of the grating and of the model could be retrieved despite this realistic level of noise.

A. Post-Fabrication Telemetry

1. Grating Parameters

The grating parameters would have to be determined before any dielectrics is deposited. A natural way of determining these geometrical parameters would be to rely on a scanning electron microscope (SEM) or an atomic force microscope (AFM), which would both allow one to directly measure the precise parameters for each of the grooves of the grating. However, for a structure without any dielectrics, the impact of nonlocality is negligible—which means that the geometrical parameters can be determined using telemetry, without any assumption on the nonlocal parameter, i.e., with a local model. The optical response of a grating actually depends more on *average* geometrical parameters [72], as the grooves may be all slightly different. Telemetry has the advantage of allowing the determination of these average parameters (especially the period of the grating), which will constitute our geometric model.

We generate an artificial measurement spectrum that we denote as $R_{\text{meas}}(\lambda)$. Furthermore, it is possible for given d_G, a_G, and h_G to compute a theoretical spectrum $R(\lambda)$. We define the distance between the two spectra as

$$\| R_{\text{meas}}(\lambda) - R(\lambda) \|^2_{L^2(\lambda_1,\lambda_2)} = \int_{\lambda_1}^{\lambda_2} (R_{\text{meas}}(\lambda) - R(\lambda))^2 \mathrm{d}\lambda. \tag{14}$$

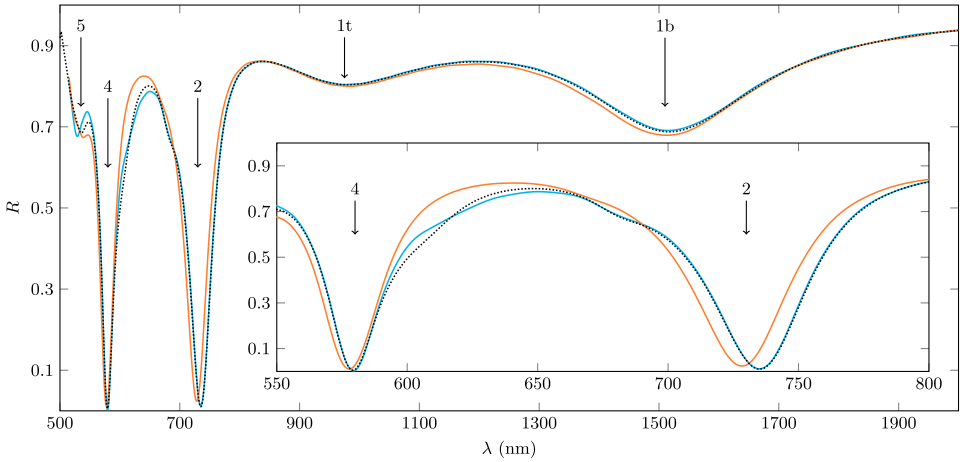

Fig. 6. Reflectivity R of the whole structure as a function of the wavelength λ. The orange line corresponds to the nonlocal DGTD result, the blue line to the local DGTD result, and the black, dotted line to the local RCWA result. The annotations 1t, 1b, 2, 4, and 5 refer to the excitation of the SP with respect to the diffraction order m of Eq. (13). The inset plot zooms in to the wavelength range of 550–800 nm, where the impact of nonlocality is the most prominent.

The integration interval $[\lambda_1, \lambda_2]$ will be chosen differently in the following, depending on which parameters have to be retrieved. We performed multiple optimization runs with different algorithms (particle swarm, pattern search, and a derivative-based optimizer combined with a kriging-based meta-model) in order to find the parameters (d_G, a_G, and h_G), which would produce the minimum distance between the theoretical spectrum and the artificially generated one. We underline that we constrained the optimization to look for geometrical parameters in intervals that would be in accordance with the precision of the etching process. The fabrication tolerances of state-of-the-art nano-processing still lead to *a priori* tolerances of about ± 5 nm for the etching process [73] and about $\pm 11\%$ [74] for the dielectric deposition.

Considering spectra between 400 nm and 1200 nm to retrieve the parameters, we have found that the derivative-based optimization method performed best, followed by pattern search and particle swarm, the latter seemingly being less appropriate for this type of optimization problem. The geometrical parameters could be retrieved with an excellent accuracy despite the noise (see Fig. 7).

2. Dielectric Thickness

The dielectric thickness has to be determined by telemetry. While the previous step can be performed with purely local simulations, here nonlocality clearly plays a role. This time, our artificially measured data are generated using the nonlocal spectrum corresponding to the right part of Fig. 6, i.e., $[\lambda_1, \lambda_2] = [800, 2000]$ nm. Since the resonances 1t and 1b are almost insensitive to nonlocality, trying to retrieve h_D by minimizing the distance between the measured nonlocal spectrum and a local in this wavelength range makes sense and actually yields results that are very close to the real value (the retrieved value was $h_D = 84.8$ nm, with the real value being $h_{D,init} = 85$ nm).

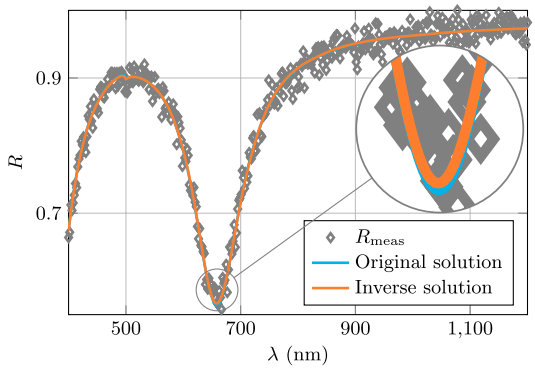

Fig. 7. Reflectivity spectrum. An artificial white noise has been added to the original spectrum (in blue) obtained for a grating illuminated in normal incidence without any dielectric layer and with $h_G = 68.0$ nm, $d_G = 500.00$ nm, and $a_G = 166.7$ nm. In orange: the result of the optimization. This spectrum corresponds to $h_G = 68.1$ nm, $d_G = 499.2$ nm, and $a_G = 165.4$ nm. The constraint intervals are chosen to be $h_G \in [62, 73]$ nm, $d_G \in [495, 505]$ nm, and $a_G \in [161, 171]$ nm.

B. Geometric Uncertainty versus Nonlocality

The geometric telemetry has led to the fabricated geometries in Table 1, where, for each parameter z with initial values z_{init} used to create R_{meas}, $\overline{z} = z_{opt}$ is the mean value and $\delta_z = |\overline{z} - z_{init}|$ the maximum deviation.

Given the uncertainties due to the retrieval process (with other means of measuring the geometric parameters, these uncertainties would likely be of the same magnitude), we need to be sure that we will be able to distinguish the impact of nonlocality from an unavoidable small error in the determination of the geometric parameters. We use UQ to provide us with answers, and in order to estimate the impact of nonlocality, we use, again, a β value from the literature [39].

We recast the geometrical parameters h_G, d_G, a_G, and h_D as random variables (RVs) following uniform distributions

Table 1. Uncertain Parameters Extracted from Telemetry

Parameter	$\bar{z}$	δ_z	Units
h_G	68.1	0.1	(nm)
d_G	499.2	1.0	(nm)
a_G	165.4	1.5	(nm)
h_D	84.8	0.3	(nm)

$\mathcal{U}[\bar{z}-\delta_z, \bar{z}+\delta_z]$ [see Table 1]. We then perform an UQ [75] study, in order to estimate the expectation value and variance of the reflectivity in two resonance regions corresponding to the diffraction orders 2 and 4. In particular, we consider 25 wavelengths in the range of [550,600] nm ($m=4$) and 50 wavelengths in the range of [700,800] nm ($m=2$).

Since the underlying computational model is a complex one, we rely on black-box UQ methods, i.e., the model and its numerical solvers are used without any modifications. In the context of the present work, we employ a spectral method [76,77], in particular the stochastic collocation method [78–80], taking advantage of a number of factors. First of all, we deal with a small number of RVs; therefore, the costs of the method remain affordable. Moreover, numerical tests indicate that the dependence of the reflectivity upon the RVs is smooth, which is a prerequisite for fast convergence. Finally, we assume that the RVs are mutually independent, which greatly simplifies the method's implementation.

The first step is to choose M different sets of values for the geometrical parameters $\mathbf{z}=(h_G, d_G, a_G, h_D)$, called the collocation points. For each wavelength mentioned above, the reflectance $R(\lambda)$ can be considered as a function $f(z)$, which is approximated by

$$f(\mathbf{z}) \approx \sum_{m=1}^{M} f(\mathbf{z}^{(m)})\Psi_m(\mathbf{z}), \tag{15}$$

where $\mathbf{z}^{(m)}$ are realizations of the random vector (the collocation points) and Ψ_m are multivariate Lagrange polynomials. The collocation points are based on univariate Clenshaw-Curtis quadrature nodes and are produced by Smolyak sparse grid rules [81,82]. The multivariate polynomials are formatted as products of univariate Lagrange polynomials, defined by the corresponding univariate Clenshaw-Curtis nodes.

The reflectivity's expectation value $\mathbb{E}[R]$ and variance $\mathbb{V}[R]$ can now be estimated by post-processing the approximation terms of Eq. (15). Starting with the definitions

$$\mathbb{E}[R] = \int_{\Gamma} f(\mathbf{z})\rho(\mathbf{z})\mathrm{d}\mathbf{z}, \tag{16}$$

$$\mathbb{V}[R] = \mathbb{E}[(R-\mathbb{E}[R])^2] = \mathbb{E}[R^2] - (\mathbb{E}[R])^2, \tag{17}$$

where $\rho(\mathbf{z})$ is the joint probability density function, we approximate the corresponding integrals with the multi-dimensional Gauss quadrature formulas

$$\mathbb{E}[R] \approx \sum_{m=1}^{M} w_m f(\mathbf{z}^{(m)}), \tag{18}$$

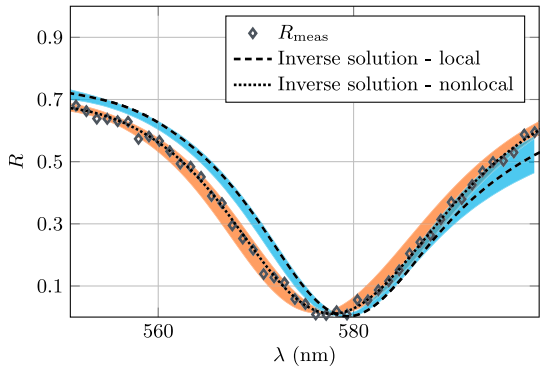

Fig. 8. Comparison of the local and nonlocal reflectivity for diffraction order $m=4$. The positions of the local resonances are 579 nm, and 577 nm for the nonlocal one. This leads to a blue shift of almost 2 nm. In blue: the $\mathbb{E}[R]\pm 2\sigma$ area, being an output of the UQ analysis based on a stochastic collocation method. In orange: the min-max intervals of the reflectivity for all interval bound combinations of the geometrical parameters given in Table 1.

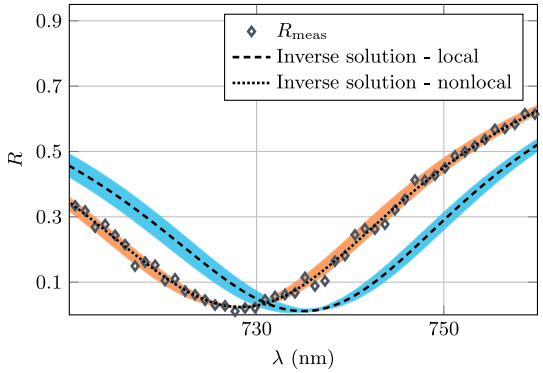

Fig. 9. Same as Fig. 8 for order of diffraction $m=2$. The positions of the local resonances are 735 nm, and the nonlocal ones are 728 nm. This leads to a blue shift of almost 7 nm.

$$\mathbb{V}[R] \approx \sum_{m=1}^{M} w_m (f(\mathbf{z}^{(m)}) - \mathbb{E}[R])^2, \tag{19}$$

where w_m denote the corresponding quadrature weights. We use the UQ study results in order to estimate $\pm 2\sigma$ intervals around the optimized local reflectivity curve, where $\sigma = \sqrt{\mathbb{V}[R]}$ refers to the standard deviation. The results corresponding to each resonance area are presented in Figs. 8 and 9 (in blue), respectively. Since the nonlocal DGTD simulations are too expensive for an UQ of the same kind as we have performed for the local model, i.e., the evaluation of Eqs. (18) and (19), we rely on a min-max study. Here, min-max represents solver calls for all interval bound combinations (in orange), as depicted in the corresponding figures.

According to Fig. 8, a clear measurement of the resonance $m=4$ is almost impossible due to the small difference between the local and nonlocal curves. Nevertheless, the second resonance, i.e., $m=2$ (see Fig. 9), is significantly more sensitive to nonlocality and stays distinguishable. For the sake of

robustness, we have also performed simulations (data not shown) with the lowest theoretically acceptable value for $\beta = 0.85 \times 10^6$ m · s^{-1} [83], which still guarantees a blue shift of 5 nm for the second resonance, i.e., stronger than the geometric uncertainty.

Other geometrical parameters could be taken into account using this approach, such as rounded corners or slanted walls. We underline that the most critical parameter would remain, in any case, the average periodicity of the grating. This parameter determines mainly the different wavevectors that are excited. We thus expect the discrepancy between the local and nonlocal simulation, which allows one to determine β to persist despite the eventual imperfections of the grating.

C. Model Calibration

Knowing the geometry and estimating the impact of nonlocality to be greater than geometric uncertainties, we now want to extract the nonlocal material parameter β. We underline that different theoretical expressions can be found in the literature for this constant [43,49,83], so that the theoretically acceptable values for β may lie between $\beta_{\min} \approx 0.85 \times 10^6$ m · s^{-1} [83] and $\beta_{\max} \approx 1.4 \times 10^6$ m · s^{-1} [43]. However, the experimental results available so far [39,40] point consistently towards a value close to the upper estimation of $\beta = 1.35 \times 10^6$ m · s^{-1}. This underlines how important the determination of β can be and explains why we have considered this value so far.

In order to estimate how precise our estimation of β can be with the grating setup, we proceed in the same fashion as for the geometric telemetry but we use a wavelength range of [550,800] nm. Using DIOGENeS and DGTD [38], we find the β value that minimizes the distance between R and R_{meas}. The geometric size of the structure, in combination with the very small effective wavelengths and the short interaction range of nonlocal effects, which is in the range of several nm at the metallo-dielectric interface, results in a computationally expensive procedure. The solution of the inverse problem can be significantly accelerated by meta-model-based optimization algorithms. We have used the kriging (Gaussian process) meta-model in combination with a derivative-based optimization implementation of the FAMOSA [84] optimization toolbox. We find $\beta_{\text{inverse}} = 1.385 \times 10^6$ m · s^{-1}, which is reasonably close to the $\beta_{\text{init}} = 1.35 \times 10^6$ m · s^{-1} (the value used to generate R_{meas}), indicating that the value of β can be retrieved with an error smaller than 10%.

6. CONCLUSION

We have first shown that, in the framework of the hydrodynamic model, SPs can be sensitive enough to spatial dispersion—provided that the dielectric considered has a sufficiently high permittivity, such as TiO_2. Such a conclusion is in contrast to previous works that suggested that the impact of spatial dispersion could be too difficult to measure optically—which is true only for an interface between metal and air.

Since there is a link between such guided modes and the localized resonances of metallic nanoparticles, this leads us to expect an impact of nonlocality on essentially any metallic nanoparticle with a radius much larger than 20 nm, for which the geometry is more likely to be well controlled, buried in a high-index medium. Using Mie theory, we estimate the blue shift brought by nonlocality to be at least of 5 nm in wavelength in TiO_2, an effect that could potentially be observed experimentally.

Since high-wavevector guided modes cannot be excited using prism couplers, we have then studied how the SPs can be excited using a grating coupler. We have shown, using state-of-the-art numerical tools, that such a structure would allow the observation of spatial dispersion by means of blue-shifted resonances up to almost 7 nm (around 1% of the wavelength). Using UQ and inverse problem solving, we have identified which resonance precisely could be used to estimate the main parameter of the hydrodynamic model and shown how such an estimation could be made. We underline that such a procedure could well be applied to nanoparticles as well.

As already evoked in several earlier works [59,85,86] and clearly demonstrated in the present work, any plasmonic structure surrounded by a high-refractive-index medium such as TiO_2 will be accurately described only if spatial dispersion is taken into account.

We believe that, by proposing a structure with realistic parameters and a procedure to carefully estimate the impact of spatial dispersion, this work will pave the way for future experiments that shall give reliable answers to the community on the limits of Drude's model for plasmonics and its potential replacements.

Funding. Deutsche Forschungsgemeinschaft (GSC 233); Agence Nationale de la Recherche (ANR-13-JS10-0003).

REFERENCES

1. P. Drude, "Zur Elektronentheorie der Metalle," Ann. Phys. **306**, 566–613 (1900).
2. J. C. Maxwell, *A Treatise on Electricity and Magnetism* (Clarendon, 1881), Vol. **1**.
3. A. Moreau, C. Ciracì, J. J. Mock, R. T. Hill, Q. Wang, B. J. Wiley, A. Chilkoti, and D. R. Smith, "Controlled-reflectance surfaces with film-coupled colloidal nanoantennas," Nature **492**, 86–89 (2012).
4. X. Chen, C. Ciracì, D. R. Smith, and S.-H. Oh, "Nanogap-enhanced infrared spectroscopy with template-stripped wafer-scale arrays of buried plasmonic cavities," Nano Lett. **15**, 107–113 (2014).
5. G. M. Akselrod, C. Argyropoulos, T. B. Hoang, C. Ciracì, C. Fang, J. Huang, D. R. Smith, and M. H. Mikkelsen, "Probing the mechanisms of large purcell enhancement in plasmonic nanoantennas," Nat. Photonics **8**, 835–840 (2014).
6. A. W. Powell, D. M. Coles, R. A. Taylor, A. A. Watt, H. E. Assender, and J. M. Smith, "Plasmonic gas sensing using nanocube patch antennas," Adv. Opt. Mater. **4**, 634–642 (2016).
7. M. Ayata, Y. Fedoryshyn, W. Heni, B. Baeuerle, A. Josten, M. Zahner, U. Koch, Y. Salamin, C. Hoessbacher, C. Haffner, D. L. Elder, L. R. D. Dalton, and J. Leuthold, "High-speed plasmonic modulator in a single metal layer," Science **358**, 630–632 (2017).
8. R. Fuchs and K. L. Kliewer, "Surface plasmon in a semi-infinite free-electron gas," Phys. Rev. B **3**, 2270–2278 (1971).
9. P. J. Feibelman, "Microscopic calculation of electromagnetic fields in refraction at a jellium-vacuum interface," Phys. Rev. B **12**, 1319–1336 (1975).
10. M. Rocca, "Low-energy eels investigation of surface electronic excitations on metals," Surf. Sci. Rep. **22**, 1–71 (1995).
11. M. Rocca, L. Yibing, F. BuatierdeMongeot, and U. Valbusa, "Surface plasmon dispersion and damping on Ag (111)," Phys. Rev. B **52**, 14947–14953 (1995).

12. S. J. Park and R. E. Palmer, "Plasmon dispersion of the Au (111) surface with and without self-assembled monolayers," Phys. Rev. Lett. **102**, 216805 (2009).
13. A. Liebsch, "Surface-plasmon dispersion and size dependence of Mie resonance: silver versus simple metals," Phys. Rev. B **48**, 11317–11328 (1993).
14. A. Liebsch, "Surface plasmon dispersion of Ag," Phys. Rev. Lett. **71**, 145–148 (1993).
15. P. J. Feibelman, "Comment on "Surface plasmon dispersion of Ag"," Phys. Rev. Lett. **72**, 788 (1994).
16. A. Liebsch, "Liebsch replies," Phys. Rev. Lett. **72**, 789 (1994).
17. A. D. Boardman, *Electromagnetic Surface Modes* (Wiley, 1982).
18. F. Frostmann and R. R. Gerhardts, *Metal Optics Near the Plasma Frequency* (Springer, 1986), Vol. **109**.
19. R. Chang, H.-P. Chiang, P. Leung, and W. Tse, "Nonlocal electrodynamic effects in the optical excitation of the surface plasmon resonance," Opt. Commun. **225**, 353–361 (2003).
20. J. A. Scholl, A. L. Koh, and J. A. Dionne, "Quantum plasmon resonances of individual metallic nanoparticles," Nature **483**, 421–427 (2012).
21. S. Raza, S. I. Bozhevolnyi, M. Wubs, and N. A. Mortensen, "Nonlocal optical response in metallic nanostructures," J. Phys. Condens. Matter **27**, 183204 (2015).
22. R. Esteban, A. G. Borisov, P. Nordlander, and J. Aizpurua, "Bridging quantum and classical plasmonics with a quantum-corrected model," Nat. Commun. **3**, 825 (2012).
23. C. Ciracì, J. B. Pendry, and D. R. Smith, "Hydrodynamic model for plasmonics: a macroscopic approach to a microscopic problem," ChemPhysChem **14**, 1109–1116 (2013).
24. A. Moreau, C. Ciracì, and D. R. Smith, "Impact of nonlocal response on metallodielectric multilayers and optical patch antennas," Phys. Rev. B **87**, 045401 (2013).
25. S. Raza, T. Christensen, M. Wubs, S. Bozhevolnyi, and N. Mortensen, "Nonlocal response in thin-film waveguides: loss versus nonlocality and breaking of complementarity," Phys. Rev. B **88**, 115401 (2013).
26. C. David, N. A. Mortensen, and J. Christensen, "Perfect imaging, epsilon-near zero phenomena and waveguiding in the scope of nonlocal effects," Sci. Rep. **3**, 2526 (2013).
27. A. Wiener, A. I. Fernández-Domnguez, J. Pendry, A. P. Horsfield, and S. A. Maier, "Nonlocal propagation and tunnelling of surface plasmons in metallic hourglass waveguides," Opt. Express **21**, 27509–27518 (2013).
28. G. Toscano, S. Raza, W. Yan, C. Jeppesen, S. Xiao, M. Wubs, A.-P. Jauho, S. I. Bozhevolnyi, and N. A. Mortensen, "Nonlocal response in plasmonic waveguiding with extreme light confinement," Nanophotonics **2**, 161–166 (2013).
29. J. B. Lassiter, X. Chen, X. Liu, C. Ciracì, T. B. Hoang, S. Larouche, S.-H. Oh, M. H. Mikkelsen, and D. R. Smith, "Third-harmonic generation enhancement by film-coupled plasmonic stripe resonators," ACS Photon. **1**, 1212–1217 (2014).
30. C. Haffner, W. Heni, Y. Fedoryshyn, J. Niegemann, A. Melikyan, D. L. Elder, B. Baeuerle, Y. Salamin, A. Josten, U. Koch, C. Hoessbacher, F. Ducry, L. Juchli, A. Emboras, D. Hillerkuss, M. Kohl, L. R. Dalton, C. Hafner, and J. Leuthold, "All-plasmonic Mach-Zehnder modulator enabling optical high-speed communication at the microscale," Nat. Photonics **9**, 525–528 (2015).
31. M. P. Nielsen, X. Shi, P. Dichtl, S. A. Maier, and R. F. Oulton, "Giant nonlinear response at a plasmonic nanofocus drives efficient four-wave mixing," Science **358**, 1179–1181 (2017).
32. H. Haberland, "Looking from both sides," Nature **494**, E1–E2 (2013).
33. G. Toscano, J. Straubel, A. Kwiatkowski, C. Rockstuhl, F. Evers, H. Xu, N. A. Mortensen, and M. Wubs, "Resonance shifts and spill-out effects in self-consistent hydrodynamic nanoplasmonics," Nat. Commun. **6**, 7132 (2015).
34. C. Ciracì and F. D. Sala, "Quantum hydrodynamic theory for plasmonics: impact of the electron density tail," Phys. Rev. B **93**, 205405 (2016).
35. G. Toscano, S. Raza, A.-P. Jauho, N. A. Mortensen, and M. Wubs, "Modified field enhancement and extinction by plasmonic nanowire dimers due to nonlocal response," Opt. Express **20**, 4176–4188 (2012).
36. J. Benedicto, R. Pollès, C. Ciracì, E. Centeno, D. R. Smith, and A. Moreau, "Numerical tool to take nonlocal effects into account in metallo-dielectric multilayers," J. Opt. Soc. Am. A **32**, 1581–1588 (2015).
37. N. Schmitt, C. Scheid, S. Lanteri, A. Moreau, and J. Viquerat, "A DGTD method for the numerical modeling of the interaction of light with nanometer scale metallic structures taking into account non-local dispersion effects," J. Comput. Phys. **316**, 396–415 (2016).
38. N. Schmitt, C. Scheid, J. Viquerat, and S. Lanteri, "Simulation of three-dimensional nanoscale light interaction with spatially dispersive metals using a high order curvilinear DGTD method," J. Comput. Phys. **373**, 210–219 (2018).
39. C. Ciracì, R. T. Hill, J. J. Mock, Y. Urzhumov, A. I. Fernández-Domínguez, S. A. Maier, J. B. Pendry, A. Chilkoti, and D. R. Smith, "Probing the ultimate limits of plasmonic enhancement," Science **337**, 1072–1074 (2012).
40. C. Ciracì, X. Chen, J. J. Mock, F. McGuire, X. Liu, S.-H. Oh, and D. R. Smith, "Film-coupled nanoparticles by atomic layer deposition: comparison with organic spacing layers," Appl. Phys. Lett. **104**, 023109 (2014).
41. S. Raza, N. Stenger, S. Kadkhodazadeh, S. V. Fischer, N. Kostesha, A.-P. Jauho, A. Burrows, M. Wubs, and N. A. Mortensen, "Blueshift of the surface plasmon resonance in silver nanoparticles studied with EELS," Nanophotonics **2**, 131–138 (2013).
42. A. D. Rakic, A. B. Djurišic, J. M. Elazar, and M. L. Majewski, "Optical properties of metallic films for vertical-cavity optoelectronic devices," Appl. Opt. **37**, 5271–5283 (1998).
43. S. Raza, G. Toscano, A. P. Jauho, M. Wubs, and N. A. Mortensen, "Unusual resonances in nanoplasmonic structures due to nonlocal response," Phys. Rev. B **84**, 121412 (2011).
44. P.-O. Chapuis, S. Volz, C. Henkel, K. Joulain, and J.-J. Greffet, "Effects of spatial dispersion in near-field radiative heat transfer between two parallel metallic surfaces," Phys. Rev. B **77**, 035431 (2008).
45. R. Ruppin, "Non-local optics of the near field lens," J. Phys. Condens. Matter **17**, 1803–1810 (2005).
46. R. Ruppin and K. Kempa, "Nonlocal effects on the imaging properties of a silver superlens," Phys. Rev. B **72**, 153105 (2005).
47. A. Wiener, A. I. Fernández-Domínguez, A. P. Horsfield, J. B. Pendry, and S. A. Maier, "Nonlocal effects in the nanofocusing performance of plasmonic tips," Nano Lett. **12**, 3308–3314 (2012).
48. C. Ciracì, Y. Urzhumov, and D. R. Smith, "Effects of classical nonlocality on the optical response of three-dimensional plasmonic nanodimers," J. Opt. Soc. Am. B **30**, 2731–2736 (2013).
49. N. Crouseilles, P. A. Hervieux, and G. Manfredi, "Quantum hydrodynamic model for the nonlinear electron dynamics in thin metal films," Phys. Rev. B **78**, 155412 (2008).
50. A. A. Maradudin and D. L. Mills, "Effect of spatial dispersion on the properties of a semi-infinite dielectric," Phys. Rev. B **7**, 2787–2810 (1973).
51. S. Lanteri, C. Scheid, and J. Viquerat, "Analysis of a generalized dispersive model coupled to a DGTD method with application to nanophotonics," SIAM J. Sci. Comput. **39**, A831–A859 (2017).
52. "DIOGENeS," https://diogenes.inria.fr/.
53. R. W. Wood, "On a remarkable case of uneven distribution of light in a diffraction grating spectrum," Proc. Phys. Soc. London **18**, 269–275 (1902).
54. U. Kreibig and M. Vollmer, *Optical Properties of Metal Clusters*, Vol. **25** of Springer Series in Materials Sciences (Springer, 2013).
55. T. Klar, M. Perner, S. Grosse, G. Von Plessen, W. Spirkl, and J. Feldmann, "Surface-plasmon resonances in single metallic nanoparticles," Phys. Rev. Lett. **80**, 4249–4252 (1998).
56. M. Scalora, M. A. Vincenti, D. de Ceglia, V. Roppo, M. Centini, N. Akozbek, and M. J. Bloemer, "Second-and third-harmonic generation in metal-based structures," Phys. Rev. A **82**, 043828 (2010).
57. J. A. Scholl, A. García-Etxarri, A. L. Koh, and J. A. Dionne, "Observation of quantum tunneling between two plasmonic nanoparticles," Nano Lett. **13**, 564–569 (2013).
58. T. V. Teperik, P. Nordlander, J. Aizpurua, and A. G. Borisov, "Robust subnanometric plasmon ruler by rescaling of the nonlocal optical response," Phys. Rev. Lett. **110**, 263901 (2013).

59. S. Raza, S. Kadkhodazadeh, T. Christensen, M. Di Vece, M. Wubs, N. A. Mortensen, and N. Stenger, "Multipole plasmons and their disappearance in few-nanometre silver nanoparticles," Nat. Commun. **6**, 8788 (2015).
60. N. A. Mortensen, S. Raza, M. Wubs, T. Søndergaard, and S. I. Bozhevolnyi, "A generalized non-local optical response theory for plasmonic nanostructures," Nat. Commun. **5**, 3809 (2014).
61. R. Ruppin, "Extinction properties of thin metallic nanowires," Opt. Commun. **190**, 205–209 (2001).
62. T. Siefke, S. Kroker, K. Pfeiffer, O. Puffky, K. Dietrich, D. Franta, I. Ohlídal, A. Szeghalmi, E.-B. Kley, and A. Tünnermann, "Materials pushing the application limits of wire grid polarizers further into the deep ultraviolet spectral range," Adv. Opt. Mater. **4**, 1780–1786 (2016).
63. D. Maystre, "Diffraction gratings," Scholarpedia **7**, 11403 (2012).
64. J. Defrance, C. Lemaître, R. Ajib, J. Benedicto, É. Mallet, R. Pollès, J.-P. Plumey, M. Mihailovic, E. Centeno, C. Ciracì, D. Smith, and A. Moreau, "Moosh: a numerical swiss army knife for the optics of multilayers in Octave/Matlab," J. Open Res. Softw. **4**, e13 (2016).
65. G. Granet and B. Guizal, "Efficient implementation of the coupled-wave method for metallic lamellar gratings in tm polarization," J. Opt. Soc. Am. A **13**, 1019–1023 (1996).
66. P. Lalanne and G. M. Morris, "Highly improved convergence of the coupled-wave method for TM polarization," J. Opt. Soc. Am. A **13**, 779–784 (1996).
67. J. R. Maack, N. A. Mortensen, and M. Wubs, "Size-dependent nonlocal effects in plasmonic semiconductor particles," Europhys. Lett. **119**, 17003 (2017).
68. D. Gall, "Electron mean free path in elemental metals," J. Appl. Phys. **119**, 085101 (2016).
69. M. Dechaux, P.-H. Tichit, C. Ciracì, J. Benedicto, R. Pollès, E. Centeno, D. R. Smith, and A. Moreau, "Influence of spatial dispersion in metals on the optical response of deeply subwavelength slit arrays," Phys. Rev. B **93**, 045413 (2016).
70. L. Li and G. Granet, "Field singularities at lossless metal-dielectric right-angle edges and their ramifications to the numerical modeling of gratings," J. Opt. Soc. Am. A **28**, 738–746 (2011).
71. O. Jamadi, F. Reveret, P. Disseix, F. Medard, J. Leymarie, A. Moreau, D. Solnyshkov, C. Deparis, M. Leroux, E. Cambril, S. Bouchoule, J. Zuniga-Perez, and G. Malpuech, "Edge-emitting polariton laser and amplifier based on a ZnO waveguide," Light Sci. Appl. **7**, 82 (2018).
72. M. Kaliteevski, J. M. Martinez, D. Cassagne, and J. Albert, "Disorder-induced modification of the transmission of light in a two-dimensional photonic crystal," Phys. Rev. B **66**, 113101 (2002).
73. E. Langereis, S. B. S. Heil, H. C. M. Knoops, W. Keuning, M. C. M. van de Sanden, and W. M. M. Kessels, "In situ spectroscopic ellipsometry as a versatile tool for studying atomic layer deposition," J. Phys. D **42**, 073001 (2009).
74. Y. Chen, "Nanofabrication by electron beam lithography and its applications: a review," Microelectron. Eng. **135**, 57–72 (2015).
75. R. C. Smith, *Uncertainty Quantification-Theory, Implementation, and Applications*, Computational Science and Engineering (SIAM, 2014).
76. O. P. Le Maitre and O. M. Knio, *Spectral Methods for Uncertainty Quantification: With Applications to Computational Fluid Dynamics*, Scientific Computation (Springer, 2010).
77. D. Xiu, *Numerical Methods for Stochastic Computations: A Spectral Method Approach* (Princeton University, 2010).
78. I. Babuska, F. Nobile, and R. Tempone, "A stochastic collocation method for elliptic partial differential equations with random input data," SIAM Rev. **52**, 317–355 (2010).
79. F. Nobile, R. Tempone, and C. G. Webster, "A sparse grid stochastic collocation method for partial differential equations with random input data," SIAM J. Numer. Anal. **46**, 2309–2345 (2008).
80. D. Xiu and J. S. Hesthaven, "High-order collocation methods for differential equations with random inputs," SIAM J. Sci. Comput. **27**, 1118–1139 (2005).
81. H.-J. Bungartz and M. Griebel, "Sparse grids," Acta Numer. **13**, 147–269 (2004).
82. S. A. Smolyak, "Quadrature and interpolation formulas for tensor products of certain classes of functions," Dokl. Akad. Nauk SSSR **148**, 1042–1045 (1963).
83. K. R. Hiremath, L. Zschiedrich, and F. Schmidt, "Numerical solution of nonlocal hydrodynamic Drude model for arbitrary shaped nanoplasmonic structures using Nédélec finite elements," J. Comput. Phys. **231**, 5890–5896 (2012).
84. R. Duvigneau, "FAMOSA," http://famosa.gforge.inria.fr.
85. A. Pitelet, É. Mallet, E. Centeno, and A. Moreau, "Fresnel coefficients and Fabry-Perot formula for spatially dispersive metallic layers," Phys. Rev. B **96**, 041406 (2017).
86. A. Pitelet, É. Mallet, R. Ajib, C. Lemaître, E. Centeno, and A. Moreau, "Plasmonic enhancement of spatial dispersion effects in prism coupler experiments," Phys. Rev. B **98**, 125418 (2018).